Accurate chromosome segregation by probabilistic self-organization

Yasushi Saka[1*†], Claudiu V Giuraniuc[1] and Hiroyuki Ohkura[2†]

*Correspondence:
y.saka@abdn.ac.uk
[1]Institute of Medical Sciences, School of Medical Sciences, University of Aberdeen, Foresterhill, AB25 2ZD Aberdeen, UK
Full list of author information is available at the end of the article
†Correspondence should be addressed to YS or HO.

arXiv:1412.5955v2 [q-bio.SC] 23 Jun 2015

Abstract

Background: For faithful chromosome segregation during cell division, correct attachments must be established between sister chromosomes and microtubules from opposite spindle poles through kinetochores (chromosome bi-orientation). Incorrect attachments of kinetochore microtubules (kMTs) lead to chromosome mis-segregation and aneuploidy, which is often associated with developmental abnormalities such as Down syndrome and diseases including cancer. The interaction between kinetochores and microtubules is highly dynamic with frequent attachments and detachments. However, it remains unclear how chromosome bi-orientation is achieved with such accuracy in such a dynamic process.

Results: To gain new insight into this essential process, we have developed a simple mathematical model of kinetochore-microtubule interactions during cell division in general, i.e. both mitosis and meiosis. Firstly, the model reveals that the balance between attachment and detachment probabilities of kMTs is crucial for correct chromosome bi-orientation. With the right balance, incorrect attachments are resolved spontaneously into correct bi-oriented conformations while an imbalance leads to persistent errors. In addition, the model explains why errors are more commonly found in the first meiotic division (meiosis I) than in mitosis and how a faulty conformation can evade the spindle assembly checkpoint, which may lead to a chromosome loss.

Conclusions: The proposed model, despite its simplicity, helps us understand one of the primary causes of chromosomal instability—aberrant kinetochore-microtubule interactions. The model reveals that chromosome bi-orientation is a probabilistic self-organization, rather than a sophisticated process of error detection and correction.

Keywords: chromosome segregation; kinetochore; microtubule; mitosis; meiosis; Markov chain; self-organization

Background

Accurate segregation of chromosomes during cell division is fundamental to life. Errors in this process result in cell death or aneuploidy. Chromosome segregation is usually very accurate. However, mis-segregation occurs at a much higher frequency in cancer cells and oocytes, which is a contributing factor to cancer progression [1] and also a major cause of infertility, miscarriages and birth defects such as Down syndrome [2].

The key event for chromosome segregation is the establishment of chromosome bi-orientation, in which sister chromatids in mitosis or homologous chromosomes in meiosis attach to the microtubules from opposite spindle poles by kinetochores [3]. Each kinetochore consists of more than one hundred different proteins assembled on each centromeric DNA sequence, many of which are involved in the interaction with microtubules [4]. Chromosome bi-orientation is a very dynamic process with frequent attachments and detachments of microtubules [5, 6, 7, 8].

For proper segregation of chromosomes, all kinetochores need to attach to spindle microtubules while erroneous attachments must be eliminated before anaphase onset. It is known that attachment errors are more frequent in meiosis I (especially in oocytes) than in mitosis [5, 6, 7, 2]. Yet it has not been understood why it is so. Unattached kinetochores act as signal generators for the spindle assembly checkpoint, which delays chromosome segregation until proper bi-orientation is established for all chromosomes [9]. It remains unclear, however, whether improperly attached kMTs are also detected and corrected by the spindle assembly checkpoint or by an independent mechanism [10].

The precise mechanism of chromosome bi-orientation has been under intense investigations. However, it is not yet possible to observe the dynamics of individual microtubules in vivo in real time. Mathematical modeling provides a powerful means to study the chromosome bi-orientation process. Since the discovery of the dynamic instability of microtubules [11], a number of theoretical analyses have provided important insights into the interaction between microtubules and kinetochores (for example, [12, 13]). The so-called search-and-capture model explains how dynamically unstable microtubules capture chromosomes [14, 15, 16, 17]. However, the original search-and-capture model did not concern events after capture, in particular, erroneous attachments of kMTs and their correction. To address this, Paul et al. put forward a modified search-and-capture model with explicit correction mech-

anisms [18]. Gay et al. proposed a stochastic model of kinetochore-microtubule attachments in fission yeast mitosis, which reproduced correct chromosome bi-orientation and segregation in simulations [19]. In addition to the kinetochore-microtubule interaction, Silkworth *et al.* showed that timing of centrosome separation also plays a crucial role for accurate chromosome segregation [20]; using experimental and computational approaches they demonstrated that cells with incomplete spindle pole separation have higher rate of kMT attachment errors than those with complete centrosome separation. Yet, the question remains unanswered as to how the cell can discriminate between correct and incorrect kMT attachments as their models assumed an explicit bias based on the discrimination of correct versus incorrect connections.

A major impediment to fully understanding the mechanism of chromosome bi-orientation is the lack of a universal theoretical framework that covers the chromosome bi-orientation process during eukaryotic cell divisions in general, including both mitosis and meiosis. Here we present such a universal model of chromosome bi-orientation, which is simple yet applicable to any eukaryotic cell division. Firstly, the model reveals that the balance between attachment and detachment probabilities of kMTs is crucial for correct chromosome bi-orientation. With the right balance, incorrect attachments are resolved spontaneously into correct bi-oriented conformations while an imbalance leads to persistent errors. Therefore, the superficially complex process, chromosome bi-orientation, is in fact a probabilistic self-organization. It implies that the cell does not need to discriminate between correct and incorrect kMT attachments. Moreover, the model explains why errors are more frequent in meiosis I than in mitosis and how a faulty conformation can evade the spindle assembly checkpoint by a gradual increase of the number of kMTs. Despite its simplicity, the model is consistent with a number of experimental observations and provides theoretical insights into the origins of chromosomal instability and aneuploidy.

Results and discussion

A probabilistic model of kinetochore-microtubule interaction

A single kinetochore can bind randomly to microtubules from either left or right pole (Fig. 1A). We assume a single kinetochore can accommodate up to n microtubules. The process of microtubule attachment/detachment can be represented as a discrete-time Markov chain [21] (Figs. 1B and S1). Each pair of sister chromatids in mitosis has two kinetochores (k_1

and k_2 in Fig. 1C). In meiosis I, a pair of sister kinecotochores are physically connected side-by-side and act as one [22, 23]. Therefore, in our model, a bivalent (a pair of homologous chromosomes connected by chiasma) also has two kinetochores in meiosis I. We assume these two kinetochores interact with microtubules independently. Hence, the state of the kinetochores is represented as $r_n(i_1, j_1, i_2, j_2)$, which can be classified into one of five classes according to the pattern of microtubule attachments (Fig. 1D). State transitions occur in a stereotypical manner among these classes irrespective of the value of $n \geq 2$ (Figs. 1E and S2E; refer to Table 1 for summary of parameters herein). Notably, the only possible transitions out of class 5 (amphitelic, i.e. correct conformation) is to class 2 (monotelic) or 4 (merotelic) (red and green arrows in Fig. 1E). Note also that this transition scheme is similar to the 'kinetic error correction' model (a deterministic ODE model) proposed by Mogilner and Craig [24]; their scheme is a limiting case—only two kMT attachments per kinetochore are allowed and transitions out of amphitelic states are prohibited.

We assume the association probability is proportional to the available surface area of the kinetochore while the dissociation probability is independent, as illustrated below:

$$r_n(i_1, j_1, i_2, j_2) \xrightarrow{\frac{n-i_1-j_1}{n}p} r_n(i_1+1, j_1, i_2, j_2), \tag{1}$$

$$r_n(i_1, j_1, i_2, j_2) \xrightarrow{i_1 q} r_n(i_1-1, j_1, i_2, j_2), \tag{2}$$

where $0 \leq p \leq 1/4$ and $0 \leq q \leq 1/2n$. $2 \times p$ is the association probability of a single microtubule to a free kinetochore; q is the dissociation probability of a single kMT.

Experimental evidence strongly suggests that tension stabilises the spindle attachment to the kinetochores in amphitelic states (class 5) [25, 26, 27]. The stabilisation by tension is brought about by suppression of Aurora B kinase activity towards kinetochore substrates [28, 29, 27, 30] as well as by mechanical 'catch-bonds' [31, 32]. We model this stabilisation by scaling the transition probabilities of states in class 5 by detachment with the parameter $0 \leq \beta \leq 1$ (Fig. 1F). This rule also reduces the probability of transitions from class 5 to class 2 states (Fig. 1E, red arrow). Similarly, the probability of class 5 (amphitelic) to class 4 (merotelic) transitions, which occur by attachment of a microtubule but not by detachment (Fig. 1E, green arrow), scales with $0 \leq \alpha \leq 1$ (Fig. 1F). This is due to the physical constraint imposed in amphitelic states in meiosis I [6, 7] or the kinetochore geometry (back-to-back position of sister kinetochores) in mitosis [3]. In mitosis, $\alpha = 0$ for simplicity. For mitosis we

introduce an additional parameter $0 \leq \gamma \leq 1$ to scale the transition probabilities from class 2 (monotelic) to class 3 (syntelic) or 4 (merotelic) (Fig. 1e, blue arrows). This is because the biased orientation of sister kinetochores hinders those transitions (Fig. 1F). Note that when $\alpha = \beta = 0$, transitions out of class 5 are effectively blocked; hence, this Markov process always ends up in class 5. For additional details of the model, see Supplementary Information (SI) Text. This simple model, which has only six parameters and is exactly solvable, provides a number of analytical insights into how correct chromosome bi-orientation is achieved.

Dynamics of chromosome bi-orientation process

The model predicts how long it takes to reach class 5 (amphitelic) from class 1 (free), i.e. mean first passage time [33] (see SI Text). For a given value of q, the mean first passage time (which is independent of α and β because they only affect transitions out of class 5) is shortest when p is roughly equal to q (Figs. 2A and S3A-D). Thus, the relative dissociation rate (q/p ratio) of kMTs needs to be balanced for efficient chromosome bi-orientation.

The model also predicts the dynamics of the system (Fig. 2B-D for meiosis I and E-G for mitosis). Note that the q/p ratio dictates the dynamics of the Markov chain (Fig. S5). For both mitosis and meiosis in an ideal condition ($p = q = 0.05, \alpha = \beta = 0$; Fig. 2B, E), the probability of class 5 steadily increases, asymptotically reaching 1. Notably, in meiosis I, class 4 (merotelic), and class 3 (syntelic) to a lesser extent, become transiently prominent (Fig. 2B). Merotelic attachments are indeed frequently observed in prophase to prometaphase of meiosis I in mouse oocytes [7]. By contrast, in mitosis, class 2 (monotelic) becomes predominant before replaced by class 5, although minor fractions of class 3 and 4 also appear briefly (Fig. 2E). Together, it explains why meiosis I is more error-prone than mitosis; it is attributed to the parameter γ— the back-to-back conformation of sister kinetochores, which biases the kinetochore orientation.

If there is no bias in meiosis I (random condition; $\alpha = \beta = 1$; Fig. 2C, see also Fig. S4), the probability of class 5 stays low while that of class 4 (merotelic) reaches nearly one half at steady states. This is because class 4 is by far the largest among the five classes (Fig S2A and S2B). In mitosis, when the spindle tension is lacking ($\beta = 1$; Fig. 2F), the model predicts high probability of errors, mainly monotelic (class 2) states, as well as the correct amphitelic (class 5) ones at steady states. When kinetochore-microtubule attachment is stabilised by reducing q, merotelic errors (class 4) persists in both meiosis and mitosis (Fig. 2D, G). Class

5 will eventually replace class 4 but only very slowly; in meiosis I with $p = 0.05, \alpha = \beta = 0$, the mean first passage times to class 5 are ~ 1631 for $q = 0.01$ versus ~ 47 for $q = 0.05$.

A number of studies demonstrated that experimental manipulations of kinetochore-microtubule interactions lead to accumulation of incorrect spindle attachments (class 1-4) and aneuploidy [8]. Lack of tension (i.e. $\beta = 1$) makes amphitelic states (class 5) unstable [25, 26, 27]. Conversely, inhibition or depletion of Aurora B kinase, which over-stabilizes kMT attachments (by reducing q), caused errors in chromosome alignment and segregation [34, 27, 30, 35, 7]. These observations are consistent with our model predictions in which imbalance of the q/p ratio causes persistent errors in kMT attachments (Fig. 2).

Probability distribution of the number of kMTs over time

Next, we calculated the probability distribution of the number of kMTs over time in different conditions (Figs. 3A-C and S6 for meiosis I; Fig. S7 for mitosis). We found qualitatively similar kMT distributions in mitosis and meiosis I, except the difference in the predicted phenotype in various conditions (Fig. 2B-G). The model predicts that in 'normal' conditions ($p = q = 0.05, \alpha = \beta = 0$) the number of kMTs increases steadily in class 5 while it remains low in the other classes as their total probability diminishes (Figs. 3A and S7A). This is in agreement with experimental evidence suggesting the gradual increase of kMTs during prometaphase to metaphase in mitosis [36] and in meiosis I [26]. With smaller q, the number of kMTs increases not only in class 5 but also in class 4 (Figs. 3B and S7B). This explains why errors persists in this condition. Note that when $\beta = 0$, the number of kMTs approaches n. Increasing number of kMTs may also switch off the spindle assembly checkpoint in merotelic (class 4) states over time.

These model predictions on the probability distribution of the number of kMTs have an important implication in the regulation of spindle assembly checkpoint. Experimental evidence suggests that intrakinetochore stretching (or kinetochore deformation), which is brought about by kMT attachments, has a role in relieving the spindle assembly checkpoint [37, 38, 39]. Therefore the predicted gradual increase of kMTs in amphitelic (class 5) states (Figs. 3A and S7A) may switch off the spindle assembly checkpoint progressively. The same argument applies to merotelic (class 4) states, the probability of which increases when q/p ratio is small (Fig. 2D, G); stabilisation of kMTs (Figs. 3B and S7B) may also inactivate the spindle assembly checkpoint in merotelic states over time. This provides the explanation

as to why merotelic orientation evades the spindle assembly checkpoint [40], leading to aneuploidy. Intrakinetochore stretching by kMT attachment, however, does not allow the cell to discriminate between correct (amphitelic; class 5) versus incorrect (non-amphitelic; class 1-4) kMT attachments [10]—the cell does not need to do so because chromosome bi-orientation occurs by probabilistic self-organisation as our model indicates.

We also examined how kMT number changes in amphitelic states under low spindle tension ($\beta = 1$; Figs. 3C and S7C). Regardless of the classes, the distribution of kMT number remains low, which makes the transition of the process from one class to another more frequent. Similar probability distributions of kMT number in meiosis I were obtained when $\alpha = \beta = 1$ (Fig. S6A) and $\alpha = 1, \beta = 0$ (Fig. S6B).

The exact probability distribution of kMT number at steady states can be derived in the special case when $\alpha = \beta = \gamma = 1$: its mean is $\bar{N} = n\rho/(n+\rho)$ where $\rho = 2p/q$ ($\bar{N} = 5/3$ for $p = q, n = 10$). We also obtained an analytical approximation of the kMT number distribution in class 5 when $\alpha = 0$:

$$\bar{N}_5 = \frac{\bar{\rho}\left(\frac{\bar{\rho}}{n}+2\right)^{n-1}}{\left(\frac{\bar{\rho}}{n}+2\right)^{n}-2^n}, \tag{3}$$

where $\bar{\rho} = \rho/\beta = 2p/(\beta q)$ (Figs. 3D and S8A, B). This formula is valid for both mitosis and meiosis and provides an analytical explanation as to how tension (β) alters the stability of kMTs by modulating the q/p ratio.

Dynamics of multiple chromosomes

The above results concern the behaviour of a single pair of homologous chromosomes. It is natural to ask how multiple pairs in the cell are bi-oriented simultaneously—we call this event 'synchrony' to distinguish it from anaphase onset. We assumed the system consists of k independent Markov processes. Let θ_t be the probability of a process being in class 5 (amphitelic) at time $T = t$, then the probability of synchrony at $T = t$ is ${\theta_t}^k$ (see SI Text).

The timing of synchrony delays as k increases (Figs. 4A and S3E, solid lines). If the balance of q/p ratio is broken by reducing q (Figs. 4A and S3E, dashed lines), the timing of synchrony is delayed further (see also Fig. S9). The probabilities of synchrony, however, eventually approach 1 in all of these conditions with $\beta = 0$. This implies that delaying the onset of anaphase could reduce the chromosome mal-orientation and mis-segregation.

Consistently, Cimini et al. showed that prolonging metaphase significantly reduced lagging chromosomes in anaphase (indicating incorrect kMT attachments) in mitosis [41].

We next examined the contribution of α and β to the establishment of synchrony. Fig. 4B shows the steady-state probability of synchrony in meiosis I as a contour plot. It indicates that, to achieve a synchrony reliably at steady states, α and β have to be relatively small. It is conceivable that, to progress into anaphase, synchrony has to be maintained for a sufficient time to relieve the spindle assembly checkpoint [10]. Fig. 4C depicts the half-life of synchrony in meiosis I as a contour plot (see also Fig. S3F for mitosis). The half-life increases steeply towards the small values of α and β. These data suggest that α and β need to be tightly regulated for efficient chromosome bi-orientation and segregation accuracy.

Error correction of kMT attachments in meiosis I

Finally, we asked how many rounds of error correction of kMT attachments occur in meiosis I before the establishment of correct bi-orientation (see SI Text for methods). We calculated the number of bi-orientation attempts per bivalent, i.e. the mean number of transitions from class 2 or 4 to class 5 before the kinetochore is fully occupied ($r_n(n,0,0,n)$ and $r_n(0,n,n,0)$ when $\beta = 0$) (Fig. 4D). It suggests that the larger α, the more bi-orientation attempts. We also found the number of bi-orientation attempts decreases as q (detachment probability) reduces (Fig. 4D, see also Fig. S10). Consistent with this, Kitajima et al. observed the number of attempts reduced from ~ 3 in untreated mouse oocytes to just one on average in those treated with Hesperadin, an Aurora B kinase inhibitor [7].

Conclusions

Our simple discrete-time Markov chain model captures the prominent features of chromosome bi-orientation process. It provides a unified account of two modes of divisions, mitosis and meiosis I, under a single theoretical framework; the model reveals where the differences in the bi-orientation process come from. It explains why errors are very frequent in the first meiotic division, which are major causes of infertility, miscarriages and birth defects in humans.

One of our key findings in this study is that the system dynamics (including the type and frequency of transient kMT attachment errors) is dictated by the q/p ratio (relative detachment rate) of kMTs. An imbalance of q/p ratio causes persistent attachment errors

leading to chromosome mis-segregations. The gradual increase of kMTs may help turn off the spindle assembly checkpoint in normal conditions but can promote a faulty conformation (merotelic attachments) to evade the checkpoint.

In summary, our study revealed that the chromosome bi-orientation is a probabilistic self-organization, rather than a sophisticated process of error detection and correction. Although our model omits many potentially important factors for chromosome bi-orientation, such as the spatial arrangement of centrosomes, it allowed us to examine analytically all possible outcomes with different parameters (i.e. the whole parameter space), revealing what is fundamental to accurate chromosome segregation. The proposed model, which is based on a firm mathematical foundation, gives valuable insights that help us understand one of the primary causes of chromosomal instability—aberrant kMT dynamics.

Methods

The model and its analysis are explained in detail in SI Text (Additional File 1). The analysis of discrete-time Markov chains were performed according to [21, 33, 42]. We used *Mathematica*® (version 10, Wolfram Research) for the analysis of the model, with a standard laptop (or desktop) computer. The *Mathematica* codes used in this study are provided in Additional File 2.

Competing interests

The authors declare that they have no competing interests.

Author's contributions

YS and HO designed the model; YS wrote the computer codes and analysed the model; CVG analysed the model; and all authors wrote the paper.

Acknowledgements

We thank G. Bewick, C. Grebogi, S. Hoppler, A. Lorenz, C. McCaig, F. Perez-Reche, R. Sekido, M. Thiel and E. Ullner for helpful discussions and critical reading of the manuscript. YS and CG are supported by Scottish Universities Life Sciences Alliance (SULSA) and HO by Wellcome Trust (grant number 098030 and 092076).

Author details

[1]Institute of Medical Sciences, School of Medical Sciences, University of Aberdeen, Foresterhill, AB25 2ZD Aberdeen, UK. [2]Wellcome Trust Centre for Cell Biology, University of Edinburgh, Michael Swann Building, Max Born Crescent, EH9 3BF Edinburgh, UK.

References

1. Bakhoum, S.F., Thompson, S.L., Manning, A.L., Compton, D.A.: Genome stability is ensured by temporal control of kinetochore-microtubule dynamics. Nat Cell Biol **11**(1), 27–35 (2009). doi:10.1038/ncb1809
2. Jones, K.T., Lane, S.I.R.: Molecular causes of aneuploidy in mammalian eggs. Development **140**(18), 3719–30 (2013). doi:10.1242/dev.090589
3. Tanaka, T.U.: Kinetochore-microtubule interactions: steps towards bi-orientation. EMBO J **29**(24), 4070–82 (2010). doi:10.1038/emboj.2010.294
4. Cheeseman, I.M.: The kinetochore. Cold Spring Harb Perspect Biol **6**(7), 015826 (2014). doi:10.1101/cshperspect.a015826
5. Dietz, R.: Multiple geschlechchromosomen bei den cypriden ostracoden, ihre evolution und ihr teilungsverhalten. Chromosoma **9**, 359–440 (1958)
6. Nicklas, R.B., Koch, C.A.: Chromosome micromanipulation. 3. spindle fiber tension and the reorientation of mal-oriented chromosomes. J Cell Biol **43**(1), 40–50 (1969)
7. Kitajima, T.S., Ohsugi, M., Ellenberg, J.: Complete kinetochore tracking reveals error-prone homologous chromosome biorientation in mammalian oocytes. Cell **146**(4), 568–81 (2011). doi:10.1016/j.cell.2011.07.031
8. Bakhoum, S.F., Compton, D.A.: Kinetochores and disease: keeping microtubule dynamics in check! Curr Opin Cell Biol **24**(1), 64–70 (2012). doi:10.1016/j.ceb.2011.11.012
9. Chen, R.H., Waters, J.C., Salmon, E.D., Murray, A.W.: Association of spindle assembly checkpoint component xmad2 with unattached kinetochores. Science **274**(5285), 242–6 (1996)
10. Khodjakov, A., Pines, J.: Centromere tension: a divisive issue. Nat Cell Biol **12**(10), 919–23 (2010). doi:10.1038/ncb1010-919
11. Mitchison, T., Kirschner, M.: Dynamic instability of microtubule growth. Nature **312**(5991), 237–42 (1984)
12. Hill, T.L.: Theoretical problems related to the attachment of microtubules to kinetochores. Proc Natl Acad Sci U S A **82**(13), 4404–8 (1985)
13. Zaytsev, A.V., Sundin, L.J.R., DeLuca, K.F., Grishchuk, E.L., DeLuca, J.G.: Accurate phosphoregulation of kinetochore–microtubule affinity requires unconstrained molecular interactions. The Journal of Cell Biology **206**(1), 45–59 (2014). doi:10.1083/jcb.201312107. http://jcb.rupress.org/content/206/1/45.full.pdf+html
14. Kirschner, M., Mitchison, T.: Beyond self-assembly: from microtubules to morphogenesis. Cell **45**(3), 329–42 (1986)
15. Holy, T.E., Leibler, S.: Dynamic instability of microtubules as an efficient way to search in space. Proc Natl Acad Sci U S A **91**(12), 5682–5 (1994)
16. Wollman, R., Cytrynbaum, E.N., Jones, J.T., Meyer, T., Scholey, J.M., Mogilner, A.: Efficient chromosome capture requires a bias in the 'search-and-capture' process during mitotic-spindle assembly. Curr Biol **15**(9), 828–32 (2005). doi:10.1016/j.cub.2005.03.019
17. Gopalakrishnan, M., Govindan, B.S.: A first-passage-time theory for search and capture of chromosomes by microtubules in mitosis. Bull Math Biol **73**(10), 2483–506 (2011). doi:10.1007/s11538-011-9633-9
18. Paul, R., Wollman, R., Silkworth, W.T., Nardi, I.K., Cimini, D., Mogilner, A.: Computer simulations predict that chromosome movements and rotations accelerate mitotic spindle assembly without compromising accuracy. Proc Natl Acad Sci U S A **106**(37), 15708–13 (2009). doi:10.1073/pnas.0908261106
19. Gay, G., Courtheoux, T., Reyes, C., Tournier, S., Gachet, Y.: A stochastic model of kinetochore-microtubule attachment accurately describes fission yeast chromosome segregation. J Cell Biol **196**(6), 757–74 (2012). doi:10.1083/jcb.201107124
20. Silkworth, W.T., Nardi, I.K., Paul, R., Mogilner, A., Cimini, D.: Timing of centrosome separation is important for accurate chromosome segregation. Mol Biol Cell **23**(3), 401–11 (2012). doi:10.1091/mbc.E11-02-0095
21. Norris, J.R.: Markov Chains, 1st pbk. ed edn. Cambridge University Press, Cambridge, UK (1998)
22. Goldstein, L.S.: Kinetochore structure and its role in chromosome orientation during the first meiotic division in male d. melanogaster. Cell **25**(3), 591–602 (1981)

23. Watanabe, Y.: Geometry and force behind kinetochore orientation: lessons from meiosis. Nat Rev Mol Cell Biol **13**(6), 370–82 (2012). doi:10.1038/nrm3349
24. Mogilner, A., Craig, E.: Towards a quantitative understanding of mitotic spindle assembly and mechanics. Journal of Cell Science **123**(20), 3435–3445 (2010). doi:10.1242/jcs.062208
25. Nicklas, R.B., Ward, S.C.: Elements of error correction in mitosis: microtubule capture, release, and tension. J Cell Biol **126**(5), 1241–53 (1994)
26. King, J.M., Nicklas, R.B.: Tension on chromosomes increases the number of kinetochore microtubules but only within limits. J Cell Sci **113 Pt 21**, 3815–23 (2000)
27. Dewar, H., Tanaka, K., Nasmyth, K., Tanaka, T.U.: Tension between two kinetochores suffices for their bi-orientation on the mitotic spindle. Nature **428**(6978), 93–7 (2004). doi:10.1038/nature02328
28. Biggins, S., Murray, A.W.: The budding yeast protein kinase ipl1/aurora allows the absence of tension to activate the spindle checkpoint. Genes Dev **15**(23), 3118–29 (2001). doi:10.1101/gad.934801
29. Tanaka, T.U., Rachidi, N., Janke, C., Pereira, G., Galova, M., Schiebel, E., Stark, M.J.R., Nasmyth, K.: Evidence that the ipl1-sli15 (aurora kinase-incenp) complex promotes chromosome bi-orientation by altering kinetochore-spindle pole connections. Cell **108**(3), 317–29 (2002)
30. Cimini, D., Wan, X., Hirel, C.B., Salmon, E.D.: Aurora kinase promotes turnover of kinetochore microtubules to reduce chromosome segregation errors. Curr Biol **16**(17), 1711–8 (2006). doi:10.1016/j.cub.2006.07.022
31. Akiyoshi, B., Sarangapani, K.K., Powers, A.F., Nelson, C.R., Reichow, S.L., Arellano-Santoyo, H., Gonen, T., Ranish, J.A., Asbury, C.L., Biggins, S.: Tension directly stabilizes reconstituted kinetochore-microtubule attachments. Nature **468**(7323), 576–9 (2010). doi:10.1038/nature09594
32. Sarangapani, K.K., Asbury, C.L.: Catch and release: how do kinetochores hook the right microtubules during mitosis? Trends Genet **30**(4), 150–9 (2014). doi:10.1016/j.tig.2014.02.004
33. Bertsekas, D., Tsitsiklis, J.: Introduction to Probability, ed. 2 edn. Athena Scientific, Nashua, NH (2008)
34. Hauf, S., Cole, R.W., LaTerra, S., Zimmer, C., Schnapp, G., Walter, R., Heckel, A., van Meel, J., Rieder, C.L., Peters, J.-M.: The small molecule hesperadin reveals a role for aurora b in correcting kinetochore-microtubule attachment and in maintaining the spindle assembly checkpoint. J Cell Biol **161**(2), 281–94 (2003). doi:10.1083/jcb.200208092
35. Kelly, A.E., Funabiki, H.: Correcting aberrant kinetochore microtubule attachments: an aurora b-centric view. Curr Opin Cell Biol **21**(1), 51–8 (2009). doi:10.1016/j.ceb.2009.01.004
36. McEwen, B.F., Heagle, A.B., Cassels, G.O., Buttle, K.F., Rieder, C.L.: Kinetochore fiber maturation in ptk1 cells and its implications for the mechanisms of chromosome congression and anaphase onset. J Cell Biol **137**(7), 1567–80 (1997)
37. Uchida, K.S.K., Takagaki, K., Kumada, K., Hirayama, Y., Noda, T., Hirota, T.: Kinetochore stretching inactivates the spindle assembly checkpoint. J Cell Biol **184**(3), 383–90 (2009). doi:10.1083/jcb.200811028
38. Maresca, T.J., Salmon, E.D.: Intrakinetochore stretch is associated with changes in kinetochore phosphorylation and spindle assembly checkpoint activity. J Cell Biol **184**(3), 373–81 (2009). doi:10.1083/jcb.200808130
39. Nannas, N.J., Murray, A.W.: Tethering sister centromeres to each other suggests the spindle checkpoint detects stretch within the kinetochore. PLoS Genet **10**(8), 1004492 (2014). doi:10.1371/journal.pgen.1004492
40. Cimini, D., Howell, B., Maddox, P., Khodjakov, A., Degrassi, F., Salmon, E.D.: Merotelic kinetochore orientation is a major mechanism of aneuploidy in mitotic mammalian tissue cells. J Cell Biol **153**(3), 517–27 (2001)
41. Cimini, D., Moree, B., Canman, J.C., Salmon, E.D.: Merotelic kinetochore orientation occurs frequently during early mitosis in mammalian tissue cells and error correction is achieved by two different mechanisms. J Cell Sci **116**(Pt 20), 4213–25 (2003). doi:10.1242/jcs.00716
42. Kemeny, J.G., Snell, J.L.: Finite Markov Chains. The University series in undergraduate mathematics. Van Nostrand, Princeton, N.J. (1960)

Figures

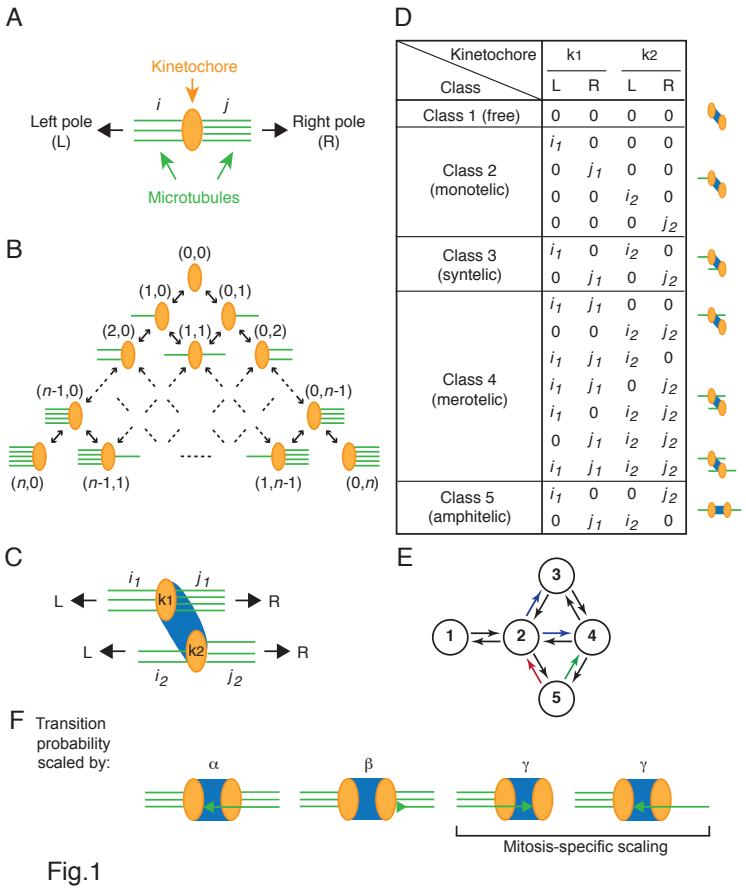

Figure 1 A discrete-time Markov chain model of kMT dynamics. (A) Schematic diagram of the interaction between a kinetochore (orange) and microtubules (green) from either left (L) or right (R) pole. i and j indicate the number of kMTs. (B) Kinetochore-microtubule interactions as a Markov chain. The maximal number of kMTs per kinetochore is n. (C) Schematic diagram of kMT dynamics during cell division. A pair of kinetochores (k1 and k2) are connected by bivalent chromatids in meiosis I or centromere chromatins (blue). (D) States of kinetochore-microtubule complex are defined with $r_n(i_1, j_1, i_2, j_2)$. Every state can be classified into one of five classes in the table. Schematic diagrams of each class are shown on the right. (E) Transition diagram among classes. A subset of states in the Markov chain categorised in (D) can move from one class to another according to this diagram. To increase the probability of class 5 states, transitions out of class 5 (red and green arrows) must be reduced, the probabilities of which are scaled with parameters α (for green arrow) and β (for red arrow) in the model. In mitosis, transitions from class 2 to class 3 or 4 are scaled with γ (blue arrows). (F) Schematic diagram of the scaling by parameters α, β and γ. Probabilities of state transition by attachment or detachment (arrowheads) are scaled by the indicated parameters.

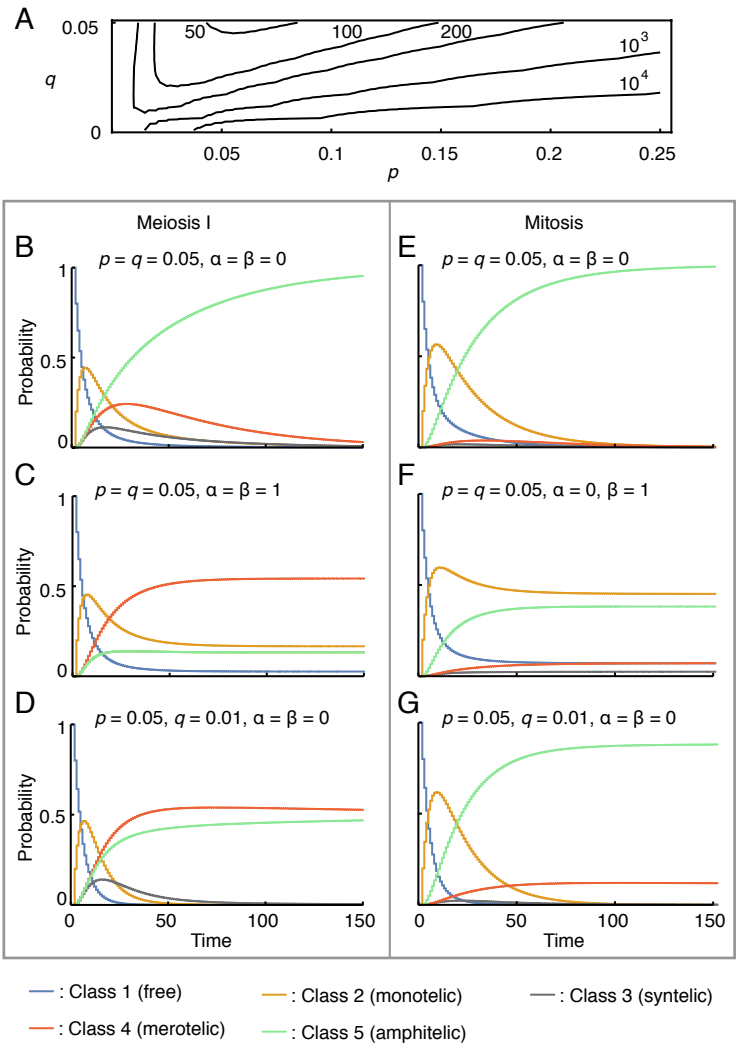

Figure 2 Dynamics of kinetochore-microtubule interaction. (A) Contour plot of mean first passage time to class 5 starting from class 1 in meiosis I. (B-G) Probabilities of each class over time for meiosis I (B-D) and mitosis (E-G). $n = 10$ for all panels. $\gamma = 1$ for meiosis I and $\gamma = 0.1$ for mitosis. Other parameters are as indicated for each panel. (B, E) An 'ideal' condition. The probability of class 5 approaches 1. (C, F) A 'random' condition with no bias towards class 5. The probability of class 4 (merotelic) becomes predominant in meiosis I (C) while class 2 (monotelic) is as prevalent as class 5 (amphitelic) in mitosis (F). Note that class 3 and class 5 have identical probabilities by symmetry in (C). (D, G) A condition in which q/p ratio is low. Class 4 persists both in meiosis I and in mitosis.

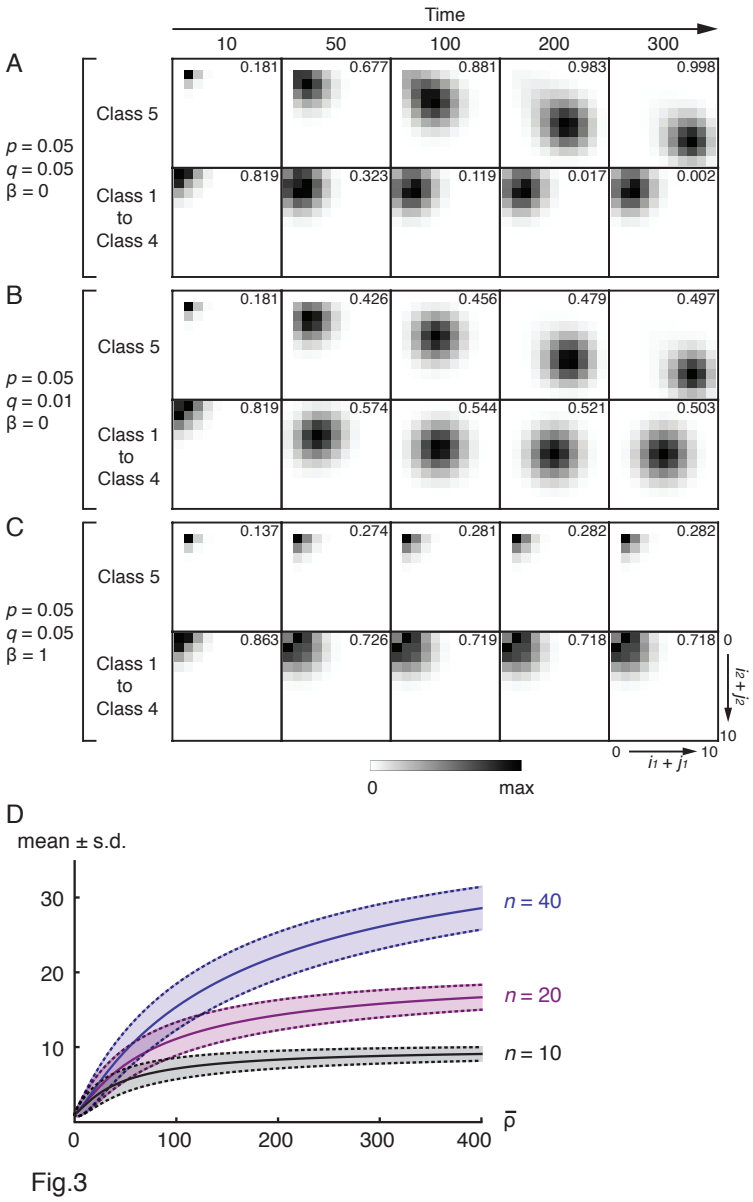

Fig.3

Figure 3 Probability distribution of the number of kMTs over time. (A-C) Probability density plots of the number of kMTs in meiosis I in 2D ($i_1 + j_1$ vs. $i_2 + j_2$; see Fig. 1C) at the indicated time points. Parameters are indicated on the left. $\alpha = 0$, $n = 10$ for all panels. Probabilities are decomposed into class 5 and the rest (class 1 to 4) at each time point. Total probabilities are indicated on each panel. The densities are scaled from 0 to the maximal for each panel. (D) Mean number of microtubules ($\pm s.d.$) attached to a kinetochore derived by the approximation formulae (Eqs. (3) and (10)). Plots for $n = 10$, 20 and 40 are shown. For details, see SI Text.

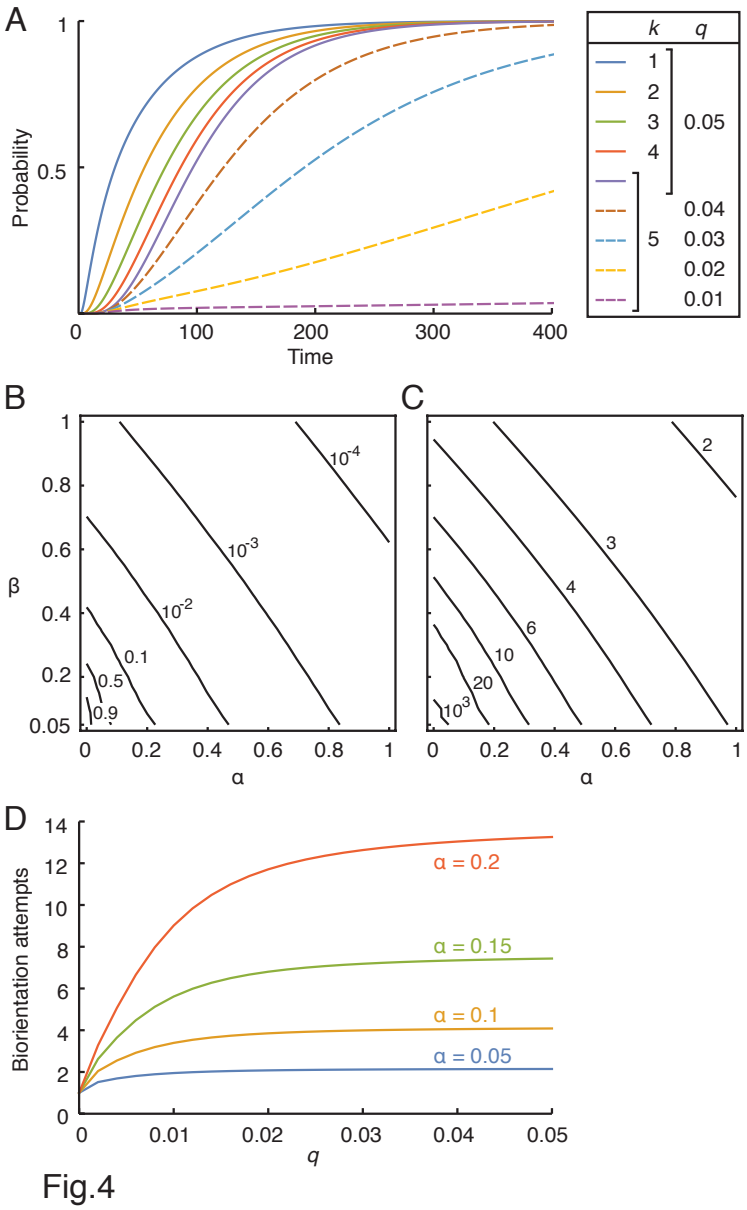

Figure 4 Dynamics of multiple chromosomes in meiosis I. (A) Probabilities of synchrony over time. k = number of chromosomes; $p = 0.05$, $\alpha = \beta = 0$. (B) Contour plot of probability of synchrony at steady states. (C) Contour plot of half-life of synchrony at steady states. In (B) and (C), $p = q = 0.05$, $k = 5$. (D) Number of biorientation attempts before absorption. $p = 0.05$, $\beta = 0$. $n = 10$ for all panels.

Tables

Table 1 Model parameters.

	Parameter for	Range of value	Biological meaning
n	Maximal number of kMTs per kinetochore	$2 \leq n$	Maximal number of kMTs that can be accommodated on a single kinetochore. n is proportional to the size of a kinetochore.
p	Association probability	$0 \leq p \leq 1/4$	$2 \times p$ is the association probability of a single microtubule to a free kinetochore in each discrete time step. Upper limit of p is $1/4$ because total probability ≤ 1.
q	Dissociation probability	$0 \leq q \leq 1/2n$	Dissociation probability of a single kMT in each discrete time step.
α	Scaling factor of p	$0 \leq \alpha \leq 1$	Scaling applies to transitions from amphitelic (class 5) to merotelic (class 4) states; reflecting the physical constraint imposed in amphitelic states (meiosis I) or the back-to-back position of sister kinetochores (mitosis). $\alpha = 0$ in mitosis for simplicity.
β	Scaling factor of q	$0 \leq \beta \leq 1$	Scaling applies to transitions in/from amphitelic states (class 5); reflecting the kMT stabilization by tension.
γ	Scaling factor of p	$0 \leq \gamma \leq 1$	Scaling applies to transitions from monotelic (class 2) to syntelic (class 3) or merotelic (class 4) states in mitosis; reflecting the biased orientation of sister kinetochores in monotelic states.

Supplementary Information

1 A basic Markov chain model of kinetochore-microtubule interactions (Model I)

The interaction of a single kinetochore with microtubules is modeled as a birth/death (discrete-time) Markov process. First, we consider a kinetochore that can bind up to n microtubules. The possible states are $M = \{0, 1, 2, ..., n\}$. Transition probability from state i to j is $p_{i,j} = P\left(X_{t+1} = j \,|X_t = i\right),\ i, j \in M$, where X_t is the state at time t. As stated in the main text, we assume the association probability is proportional to the surface area of a kinetochore available for microtubule attachment. Therefore, the association (birth) probability is $p_{k,k+1} = (n-k)\, b/n,\ 0 \leq k \leq n-1$ where b is the association probability of a single microtubule to a free kinetochore. The dissociation (death) probability for state k is $p_{k,k-1} = k\, d,\ 1 \leq k \leq n$, because each microtubule bound to a kinetochore (k microtubules in total) has the same dissociation probability d. The self-transition probability is $p_{k,k} = 1-(n-k)\, b/n - k\, d,\ 0 \leq k \leq n$. As an example, consider a kinetochore that can bind up to 2 microtubules. The possible states are $\{0, 1, 2\}$. The transition probability matrix is

$$R_3 = \begin{pmatrix} p_{0,0} & p_{0,1} & p_{0,2} \\ p_{1,0} & p_{1,1} & p_{1,2} \\ p_{2,0} & p_{2,1} & p_{2,2} \end{pmatrix} = \begin{pmatrix} 1-b & b & 0 \\ d & 1-\frac{1}{2}b-d & \frac{1}{2}b \\ 0 & 2d & 1-2d \end{pmatrix}.$$

Fig. S1A shows a diagram of this Markov chain. This model is a variation on the M/M/s queue [21]. The Markov chain consists of a single aperiodic recurrent class. Let u_k be the steady-state probabilities of state k and U be the row vector of $u_k, k = 0, 1, 2, ..., n$. Applying the steady-state convergence theorem, then $U = UR_n$. This is equivalent to a local balance equation: $(1-k/n)\, b\, u_k = (k+1)d\, u_{k+1}$. Let $\rho = b/d$ then,

$$(1-k/n)\rho u_k = (k+1)u_{k+1}, k = 0, 1, ..., n-1. \tag{4}$$

The normalization equation (the sum of all probabilities equals to 1) is

$$\sum_{k=0}^{n} u_k = 1. \tag{5}$$

Eqs. (4) and (5) yield a unique solution:

$$u_k = \binom{n}{k}(\rho/n)^k(1+\rho/n)^{-n},\ k = 0, 1, 2, ..., n, \tag{6}$$

where $\binom{n}{k}$ is the binomial coefficient ("n choose k"). When n is large, u_k approaches the Poisson distribution $e^{-\rho}\,\rho^k/\,k!$. The mean and variance of u_k, derived from Eq. (6), are $n\rho/(n+\rho)$ and $n^2\rho\,/(n+\rho)^2$, respectively. Fig. S1B shows an example of the probability distribution of u_k (the number of attached microtubules) for $n = 20$. As illustrated in this example, the stability of kinetochore-microtubule interaction can be controlled by ρ (i.e. d/b ratio) alone.

2 The extended model of kinetochore-microtubule interactions (Model II)

Now we consider the interaction of a kinetochore with bipolar spindles (Fig. 1B in the main text). There are $(n+1)(n+2)/2$ possible states, e.g. 6 possible states for $n = 2$. We assign a unique index number to each state denoted as $s_n(i, j)$:

$$s_n(i,j) \longmapsto i + 1 + \frac{(i+j+1)(i+j)}{2},\ 0 \le i+j \le n. \tag{7}$$

We use these indices to construct the probability transition matrix in *Mathematica* codes. Using the same argument for model I, the state transition probabilities are

$$\begin{aligned}
s_n(i,j) &\xrightarrow{\frac{n-i-j}{n}p} s_n(i+1,j),\\
s_n(i,j) &\xrightarrow{\frac{n-i-j}{n}p} s_n(i,j+1),\\
s_n(i,j) &\xrightarrow{i\,q} s_n(i-1,j),\\
s_n(i,j) &\xrightarrow{j\,q} s_n(i,j-1),
\end{aligned} \tag{8}$$

where p, q are parameters with $0 \leq p \leq 1/2$, $0 \leq q \leq 1/n$. For example, the transition matrix P_n with $n = 2$ is

$$P_2 = \begin{pmatrix} 1-2p & p & p & 0 & 0 & 0 \\ q & 1-p-q & 0 & \frac{p}{2} & \frac{p}{2} & 0 \\ q & 0 & 1-p-q & 0 & \frac{p}{2} & \frac{p}{2} \\ 0 & 2q & 0 & 1-2q & 0 & 0 \\ 0 & q & q & 0 & 1-2q & 0 \\ 0 & 0 & 2q & 0 & 0 & 1-2q \end{pmatrix}.$$

Model II is fundamentally the same as Model I: b in Model I is equal to the combined probability of a microtubule binding to a free kinetochore ($= 2 \times p$) in Model II. Dissociation probability of a single kMT is the same ($d = q$). Hence $\rho = 2p/q$.

3 The model of kinetochore-microtubule interactions in meiosis and mitosis (Model III)

The model of kinetochore-microtubule interactions in meiosis and mitosis is built from Model II, which we call Model III. This model describes the state of a pair of kinetochores physically connected by a centromere chromatin (in mitosis and meiosis II) or a bivalent (in meiosis I) of homologous chromosomes, which is defined by $r_n\,(i_1, j_1, i_2, j_2)$. Note that $0 \leq p \leq 1/4$ and $0 \leq q \leq 1/2n$ in Model III because the total transition probability from a given state including self-transition is 1. Also note that there is no direct transition from class 1 (free) to class 5 (amphitelic, i.e. correct conformation).

As briefly mentioned in the main text, spindle tension stabilises the kMT attachments in amphitelic states (class 5), which is represented by the scaling with the parameter β. This applies to both mitosis and meiosis. The scaling with the parameter β is exemplified by

$$r_n(i_1, 0, 0, j_2) \xrightarrow{i_1 \beta\, q} r_n(i_1 - 1, 0, 0, j_2).$$

This rule also reduces the probability of transitions from class 5 to class 2 states (red arrow in Fig. 1E; with $i_1 = 1$ in the above example).

The scaling of the probability of class 5 (amphitelic) to class 4 (merotelic) transitions with the parameter α is based on the experimental evidences. In amphitelic states in mitosis, the kinetochore geometry in mitotic chromosomes prevents each sister kinetochore from

interacting with the microtubules from the opposite pole [3]. Therefore class 5 (amphitelic) to class 4 (merotelic) transitions are effectively eliminated in mitosis, i.e. $\alpha = 0$. In meiosis I, Nicklas suggested that the stability of amphitelic conformation is also gained by the aligned position of kinetochores with the pole-to-pole axis, with each kinetochore pointing at a pole [6]. A recent study of meiosis I in mouse oocyte indeed revealed the restricted movement of kinetochores in amphitelic states (see supplemental movies in Kitajima et al [7]). The scaling with the parameter α is exemplified by

$$r_n(i_1, 0, 0, j_2) \xrightarrow{\frac{n-i_1}{n}\alpha\, p} r_n(i_1, 1, 0, j_2).$$

With a similar reason transitions from class 2 (monotelic) to class 3 (syntelic) or 4 (merotelic) are reduced in mitosis because the attached sister kinetochore are facing towards the pole from which the kMT emanates, while the other unattached sister kinetochore are facing the opposite pole. Thus, these transitions (blue arrows in Fig. 1E) are scaled by the parameter $0 \leq \gamma \leq 1$. For example,

$$\begin{aligned} r_n(i_1, 0, 0, 0) &\xrightarrow{\gamma\, p} r_n(i_1, 0, 1, 0), \\ r_n(i_1, 0, 0, 0) &\xrightarrow{\frac{n-i_1}{n}\gamma\, p} r_n(i_1, 1, 0, 0). \end{aligned}$$

These scaling of the transitions by γ are unique to mitosis (and meiosis II); for meiosis I, $\gamma = 1$.

With sufficiently small α and β, class 5 becomes stable; when $\alpha = \beta = 0$, transitions out of class 5 are not possible. That means class 5 is an absorbing class in the Markov chain. This bias towards class 5 underpins the probabilistic self-organisation of the system. By contrast, when $\alpha = \beta = 1$ there is no bias towards class 5, that is, amphitelic states are unstable. Note that when $\alpha \neq 0, \beta = 0$, the process eventually ends up in either $r_n(n, 0, 0, n)$ or $r_n(0, n, n, 0)$, that is, the class 5 states with maximal number of kMTs.

4 Steady-state PMF (probability mass function) in Model II

To calculate the steady-state PMF in Model II, consider it as a process of choosing the number of microtubules per kinetochore and distributing them to left and right poles. Let $k(\leq n)$ be the total number of microtubules attached to the kinetochore and $\phi_n(i, j)$ be the PMF for state $s_n(i, j)$, then $\sum_{i=0}^{k} \phi_n(i, j) = u_k,\ i + j = k$. $\phi_n(i, j)$ is derived by distributing

u_k according to the binomial distribution:

$$\binom{i+j}{i}(1/2)^i(1/2)^j = \binom{k}{i}(1/2)^k,\ 0 \le i \le k.$$

Hence, using Eq. (6),

$$\begin{aligned}\phi_n(i,j) &= u_k \times \binom{k}{i}(1/2)^k \\ &= \left(1+\frac{\rho}{n}\right)^{-n}\left(\frac{\rho}{2n}\right)^{i+j}\frac{n!}{i!j!(n-i-j)!}.\end{aligned} \tag{9}$$

Let $\Phi_n = (\phi_n(0,0), \phi_n(0,1), \phi_n(1,0), \phi_n(0,2), \phi_n(1,1), ..., \phi_n(n-1,1), \phi_n(n,0))$. Then, by applying Eq. (8) and (9), we find $\Phi_n.P_n = \Phi_n$, which is consistent with the equilibrium at steady states.

5 Size of the Markov chains

The size of a Markov chain in Model II (total number of states) corresponds to the maximum of the $s_n(i,j)$ indices according to Eq. (7), which is $(n+1)(n+2)/2$. The total number of states in the full model (Model III) is thus $(n+1)^2\ (n+2)^2/\,4$, which grows rapidly as n increases (Fig. S2A). Note that class 4 becomes predominant as the system size gets larger (Fig. S2B). Consequently, the number of possible state transitions also increases exponentially with the system size (Fig. S2C), which corresponds to the number of non-zero entries in the probability transition matrix.

6 First passage time to class 5

For a Markov chain of Model III, the mean first passage time f_i to class 5 from state i is obtained as the solution of linear equations [33]:

$$f_i = \begin{cases} 1 + \sum\limits_{j \notin \text{class } 5} p_{i,j} f_j, & i \notin \text{class } 5, \\ 0, & i \in \text{class } 5. \end{cases}$$

f_1 in Fig. 2A was calculated by incrementing p and q by 0.005 (50×10 points) and in Figs. S3A and S3D by 0.0001 (100×100 points). For a given value of q ($= 0.0005$), the minimum f_1 plateaus as n grows (Fig. S3B), although the number of states and transitions increase rapidly (Figs. S2A and S2C). For meiosis I, the q/p ratio for the minimum f_1 approaches

$\sim$1 as n increases (Fig. S3C). For mitosis, the optimal q/p ratio is somewhat skewed (Fig. S3D).

7 PMF time series of $r_n\,(i_1, j_1, i_2, j_2)$

It is straightforward to calculate the PMF of $r_n\,(i_1, j_1, i_2, j_2)$ at each time point from the transition probability matrix. We classified the PMFs according to Fig. 1D and calculated the sums for each class to obtain Fig. 2B to G. Fig. S4 shows the PMF time series in meiosis I with $\alpha = 0, \beta = 1$ (a) and $\alpha = 1, \beta = 0$ (b) ($n = 10, p = q = 0.05$). Class 4 is predominant in these condition as well.

The dynamics are qualitatively very similar with any n; this is mainly because the structure of the Markov chain remains the same as the size of the chain grows (Fig. 1B and S2E). We have used $n = 10$ for most of the analysis as a representative value. We extensively explored the dynamics with different values of n and found fundamentally no diffence in the behavior of the Markov chain by altering n (for example, $n = 10$ versus 15 in Figs. S5B, C, E and F).

8 Invariant dynamics of the Markov process with constant q/p ratio

As long as q/p ratio (relative kMT dissociation rate) remains the same, the steady-state probabilities of $r_n\,(i_1, j_1, i_2, j_2)$ stay the same for all p, q pairs. The PMF time series are also almost invariable (but with different time scales) as long as q/p ratio remains constant, illustrated by the examples shown in Fig. S5. Only the time scale changes, which is inversely proportional to $\sqrt{p\,q}$. Strictly speaking, although steady-state probabilities are identical, PMFs at any given moment are not exactly the same: these small differences come about by the assumption that only a single event happens in every state transition. Differences are small enough to be ignored when p and q are sufficiently small. From a biological perspective, the change in time scale with the same dynamics has a different meaning: the faster the association and dissociation of kMTs, the more efficient the chromosome biorientation. See also the section 'Biorientation attempts' below.

9 Probability distribution of kMTs at steady states in meiosis I.

Class 5

Steady state probability distributions of the number of kMTs in class 5 for $n = 10,\ p = 0.1,\ q = 0.05$ are shown in Fig. S8B as density plots. Total probability of class 5 is indicated for each panel. Gray scale is normalized to the total probability of class 5. When α and

β are sufficiently small, class 5 (amphitelic) states are stable, i.e. the number of kMTs are close to the maximum. Otherwise, only a few microtubules on average are attached to each kinetochore.

Class 1 to 4

Steady state probability distributions of the number of kMTs in classes 1 to 4 for $n = 10$, $p = 0.1$, $q = 0.05$ are shown in Fig. S8C as density plots. Although the total probabilities are greatly affected by the parameters α and β, the distribution of the number of kMTs of non-class 5 states barely changes. This is presumably because the size of the non-amphitelic classes (mainly class 4) in total is significantly larger than that of class 5 (Fig. S2B), buffering the influence of class 5. Thus, $\bar{N} = n\rho/(n+\rho)$ (the exact solution in the random condition $\alpha = \beta = \gamma = 1$) is also an approximate of the steady state distribution of kMTs in meiosis I for non-amphitelic states when $\alpha \neq 1, 0 < \beta \neq 1$.

10 Number of kMTs at steady states in class 5 — an analytical approximation

When $\alpha = 0$, the number of kMTs for states in class 5 can be estimated analytically without explicitly calculating the PMF, which is computationally expensive for large n. The reason why it is possible becomes apparent by looking at the Markov chain's structure and transitions — when $\alpha = 0$, transitions from class 5 to class 2 are still possible, but not to class 4 anymore. Note that for large n the number of transitions between class 5 and class 4 is far larger than the one between class 5 and class 2 (Fig. S2D).

Because of its limited communication with other classes when $\alpha = 0$, class 5 behaves as if it is a disjoint class at steady states. Its two sub-classes (e.g. left and right square grids in Fig. S2E) have the identical probability distribution by symmetry, which can be approximated by

$$\begin{aligned}
\psi_n(i,j) &= \phi_n(i,0) \times \phi_n(0,j) \\
&= 2^{-(i+j)} u_i \, u_j \\
&= \binom{n}{i}\binom{n}{j}\left(\frac{\bar{\rho}}{2n}\right)^{i+j}\left(1+\frac{\bar{\rho}}{n}\right)^{-2n},
\end{aligned}$$

where $1 \leq i, j \leq n$ and $\bar{\rho} = \rho/\beta = \frac{2p}{\beta q}$. We now compute the conditional expectation of the number of kMTs i (or j) given the state s is in class 5:

$$\begin{aligned} E(i|s \in \text{class } 5) &= \sum_{i=1}^{n}\sum_{j=1}^{n}(\psi_n(i,j) \times i) \Big/ \sum_{i=1}^{n}\sum_{j=1}^{n}\psi_n(i,j) \\ &= \bar{N}_5. \end{aligned}$$

After a lengthy algebra, it simplifies to Eq. (3) in the main text. Similarly,

$$E\left(i^2 \middle| s \in \text{class } 5\right) = \sum_{i=1}^{n}\sum_{j=1}^{n}\left(\psi_n(i,j) \times i^2\right) \Big/ \sum_{i=1}^{n}\sum_{j=1}^{n}\psi_n(i,j).$$

After another lengthy calculation, variance of i is reduced to:

$$\begin{aligned} \text{Var}(i|s \in \text{class } 5) &= E\left(i^2 \middle| s \in \text{class } 5\right) - \left(E(i|s \in \text{class } 5)\right)^2 \\ &= \frac{\bar{\rho}\left(2+\frac{\bar{\rho}}{n}\right)^{n-2}\left(2\left(2+\frac{\bar{\rho}}{n}\right)^{n} - 2^n\left(2+\bar{\rho}\right)\right)}{\left(\left(2+\frac{\bar{\rho}}{n}\right)^{n} - 2^n\right)^2}. \end{aligned} \tag{10}$$

Eqs. (3) and (10) fit very well to the exact number of kMTs derived from the steady-state PMF (Fig. S8A). When n is small (e.g. $n = 4$), the approximation diverges a little from the exact values, but is still pretty good (not shown). The mean and variance approach n and 0, respectively, as $\bar{\rho} \to \infty$.

11 Probability of synchrony

Computing the probability of synchrony

We compute the probability of synchrony at time $T = t$, i.e. the probability that the process in every chain is in the same class (in particular class 5) at the same time. This is illustrated by an example below, which shows the state (class) transtions of each process (Ch.1 to 4) from $T = 0$ to 20. Synchrony in class 5 is highlighted in red, which occurs at $T = 18$.

	0	1	2	3	4	5	6	7	8	9	10	11	12	13	14	15	16	17	18	19	20
Ch.1	1	2	1	1	1	1	1	1	2	3	4	4	4	4	4	2	2	2	5	5	5
Ch.2	1	1	1	1	1	1	1	1	2	4	4	4	4	4	4	4	5	5	5	5	5
Ch.3	1	2	1	1	1	1	1	2	3	3	2	5	5	5	5	5	5	5	5	5	5
Ch.4	1	2	3	3	2	2	2	3	4	4	4	4	5	5	5	5	5	5	5	5	5

Let $s[t]$ be the state of a single Markov process at time $T = t$, $a_j^{(t)}$ be the probability of $s[t] = j$ and k be the total number of chains. In the above example, $k = 4$. Also let $P_s^{(t)}$

and $P_{as}^{(t)}$ be the probability of synchrony and asynchrony at $T = t$, respectively. Then,

$$\begin{aligned} P_{s}^{(t)} &= {\theta_t}^k, \\ P_{as}^{(t)} &= 1 - P_{s}^{(t)}, \\ &= 1 - {\theta_t}^k, \end{aligned} \tag{11}$$

where

$$\theta_t = P(s[t] \in \text{class } 5) = \sum_j a_j^{(t)},\ j \in \text{class } 5.$$

We used Eq. (11) for Figs. 4A and S3E. Now we consider the probability of synchrony attempts. For this, we need some events and their probabilities defined. The probability of biorientation attempts $P_{+}^{(t)}$ in a single process is

$$\begin{aligned} P_{+}^{(t)} &= P(s[t-1] \notin \text{class } 5 \wedge s[t] \in \text{class } 5) \\ &= \sum_{i,j} a_i^{(t-1)} p_{i,j},\ i \notin \text{class } 5,\ j \in \text{class } 5, \end{aligned}$$

where $p_{i,j}$ is the transition probability from state i to j. Likewise, the probability of biorientation loss $P_{-}^{(t)}$ is

$$P_{-}^{(t)} = \sum_{i,j} a_j^{(t-1)} p_{j,i},\ i \notin \text{class } 5,\ j \in \text{class } 5.$$

The probability of biorientation maintainance $P_{0}^{(t)}$ of a process is

$$\begin{aligned} P_{0}^{(t)} &= P(s[t-1] \in \text{class } 5 \wedge s[t] \in \text{class } 5) \\ &= \sum_{i,j} a_i^{(t-1)} p_{i,j},\ i \in \text{class } 5, j \in \text{class } 5. \end{aligned}$$

Let m be the number of Markov processes in class 5 at $T = t$. Note that a synchrony attempt occurs only when all m processes that are in class 5 stay in class 5 and the remaining $k - m$ processes undergo transition from non-class 5 to class 5 states. The probability of such a synchrony attempt, $P_{\text{as},s}^{(t)}$, is

$$\begin{aligned} P_{as,s}^{(t)} &= P(\text{asynchrony at } T = t-1 \wedge \text{synchrony at } T = t) \\ &= \sum_{m=0}^{k-1} \binom{k}{m} \left(P_{+}^{(t)}\right)^{k-m} \left(P_{0}^{(t)}\right)^{m}, \end{aligned}$$

where $\binom{k}{m}$ is the binomial coefficient. Note that Fig. S9A may help understand the following derivation of formulae.

The probability of synchrony maintenance $P_{s,s}^{(t)}$ is

$$\begin{aligned} P_{s,s}^{(t)} &= P(\text{synchrony at } T=t-1 \wedge \text{synchrony at } T=t) \\ &= P_{s}^{(t)} - P_{as,s}^{(t)}. \end{aligned}$$

Likewise, the probability of asynchrony maintenance $P_{as,as}^{(t)}$ is

$$\begin{aligned} P_{as,as}^{(t)} &= P(\text{asynchrony at } T=t-1 \wedge \text{asynchrony at } T=t) \\ &= P_{as}^{(t)} - P_{s,as}^{(t)}. \end{aligned}$$

The probability of synchrony loss $P_{s,as}^{(t)}$ is obtained by

$$\begin{aligned} P_{s,as}^{(t)} &= P(\text{synchrony at } T=t-1 \wedge \text{asynchrony at } T=t) \\ &= P_{s}^{(t-1)} - P_{s,s}^{(t)} \\ &= P_{s}^{(t-1)} - \left(P_{s}^{(t)} - P_{as,s}^{(t)}\right) \\ &= P_{as,s}^{(t)} - \left(P_{s}^{(t)} - P_{s}^{(t-1)}\right). \end{aligned} \tag{12}$$

$P_{s,as}^{(t)}$ can also be obtained by

$$P_{s,as}^{(t)} = \sum_{m=1}^{k} \binom{k}{m} \left(P_{-}^{(t)}\right)^{m} \left(P_{0}^{(t)}\right)^{k-m}.$$

At steady states, the conditional probability of synchrony loss given the present state is in synchrony is $P_{s,as}^{(\infty)}/P_{s}^{(\infty)}$, therefore the mean duration (half-life) of synchrony is $P_{s}^{(\infty)}/P_{s,as}^{(\infty)}$. Fig. 4C was derived by this formula.

Now we examine when the synchrony happens for the first time, i.e. the probability of the first synchrony at $T=t$, denoted by $P_{fs}^{(t)}$. With $\alpha=\beta=0$, once a process is in class 5, it is trapped in the class (i.e. $P_{s,as}^{(t)}=0$). Therefore $P_{fs}^{(t)} = P_{as,s}^{(t)}$. When α and β are small, the majority of synchrony attempts are for the first time; in addition, as k gets larger (number of processes, i.e. pairs of sister chromatids in mitosis or bivalents in meiosis I), synchrony becomes a rarer event. Thus, the probability of synchrony loss $P_{s,as}^{(t)}$ are small at

any given moment for large k and small α and β. In such a condition, it is therefore possible to approximate $P_{fs}^{(t)}$ with $\tilde{P}_{fs}^{(t)}$:

$$\begin{aligned}\tilde{P}_{fs}^{(t)} &= P_{as}^{(0)} \\ &\times \left(\prod_{\tau=1}^{t-1} P(\text{asynchrony at } T=\tau-1 \wedge \text{asynchrony at } T=\tau | \text{asynchrony at } T=\tau-1) \right) \\ &\times P(\text{asynchrony at } T=t-1 \wedge \text{synchrony at } T=t | \text{asynchrony at } T=t-1) \\ &= \left(\prod_{\tau=1}^{t-1} \frac{P_{as,as}^{(\tau)}}{P_{as}^{(\tau-1)}} \right) \times \frac{P_{as,s}^{(t)}}{P_{as}^{(t-1)}},\ t=2,3,4\ldots.\end{aligned}$$

It is apparent that for $\alpha = \beta = 0$ (therefore $P_{s,as}^{(t)} = 0$), $\tilde{P}_{fs}^{(t)} = P_{as,s}^{(t)}$. Fig. S9B shows an example of $\tilde{P}_{fs}^{(t)}$ together with Monte Carlo simulation results (probability in 5,000 simulations), demonstrating a good fit of the approximation to the simulation result.

Timing of first synchrony and q/p ratio

We asked how q/p ratio affects the timing of first synchrony. We also asked how efficiently synchrony can be achieved in a slightly compromized condition, i.e. $\alpha = \beta = 0.05$. Fig. S9C shows the probability of first synchrony in meiosis I at each time point with decreasing q value ($n = 10$, $p = 0.05$ and the number of bivalents $k = 5$). When $p = q = 0.05$, first synchrony happens most frequently around $T = 100$; By $T = 400$ synchrony takes place at least once in $\sim 99.7\%$ of cases (not shown). As q/p ratio declines, the timing of first synchrony spreads more and more over time, becoming unpredictable. Therefore, synchrony does happen relatively efficiently with the right q/p ratio even in a slightly compromized condition with $\alpha = \beta = 0.05$. For a fixed value of $p = 0.05$, the probability of synchrony at steady state (at any give moment) is 0.66 with $q = 0.05$, but only 0.017 when $q = 0.01$. For $k = 20$, the probability declines to 0.19 with $q = 0.05$ and 8.3×10^{-8} with $q = 0.01$. Thus, keeping the balance of q/pratio is all the more important for the cell with a large number of chromosomes. This principle applies to both mitosis and meiosis I.

12 Bi-orientation attempts

Probability of bi-orientation attempts

Probability of biorientation attempts at time $T = t$, μ_t, is

$$\mu_t = \sum_{i,j} a_i^{(t)} p_{i,j},\ i \notin \text{class } 5, j \in \text{class } 5,$$

where $a_i^{(t)}$ is the probability of the process in state i at time t and $p_{i,j}$ is the transition probability from state i to j. μ_t can also be interpreted as the mean number of attempts to biorientation at time t. Fig. S10A shows a plot of μ_t by this formula (analytical solution) and simulations (parameters: $n = 5, p = q = 0.01, \alpha = \beta = 0.1$; 10,000 simulations). Fig. S10B shows an example of probability time series of biorientation attempts, with $p = q = 0.05$ versus $p = q = 0.01$ ($n = 10$, $\alpha = \beta = 0.1$). With the same q/p ratio, their PMF time series are almost identical (not shown) if the time scale is adjusted. Because of this change of time scale, the probability (i.e. frequency) of biorientation attempts also changes. In this example, the probability at steady states (at any time point) decreases from ∼0.033 with $p = q = 0.05$ to ∼0.0066 with $p = q = 0.01$.

Mean number of biorientation attempts before absorption

The number of biorientation attempts before the onset of anaphase is equivalent in our model to the total number of transitions to class 5 from either class 2 or class 4 before absorption (referred as $\bar{M}$ hereafter; Fig. 4D). This can be computed by first calculating the mean total number of times the process is in each transient state before absorption, starting from class 1. We denote this number as $M(i)$, $i \in$ (transient states). There are two absorbing states when $\beta = 0$, so the total number of transient states is $l =$ (total number of states) $- 2$. $M(i)$ is obtained from the so-called fundamental matrix N defined as $N = (I - Q)^{-1}$, where I is the $l \times l$ identity matrix and Q is the $l \times l$ submatrix of P (the transition probability matrix):

$$P = \begin{pmatrix} Q & R \\ O & S \end{pmatrix}.$$

Q defines the transition within the transient states. O is a $2 \times l$ matrix with all 0's; R concerns the transtion from transient to absorbing states; S is the 2×2 identity matrix in our model. The first row of N corresponds to $M(i)$. The formula for fundamental matrices (and also for the mean and variances of absorption time) is according to Kemeny and Snell [42]. Computing the mean of $\bar{M}$, $\langle \bar{M} \rangle$, is straightforward using $M(i)$:

$$\langle \bar{M} \rangle = \sum_i \sum_j M(i)\, p_{i,j},$$

where $i \in (\text{class2} \vee \text{class4})$, $j \in$ class 5 and $p_{i,j}$ is the transition probability from state i to j. Note that, when $\alpha = 0, \bar{M} = 1$ for all $n \geq 1$ because once in class 5 the process never leaves the class.

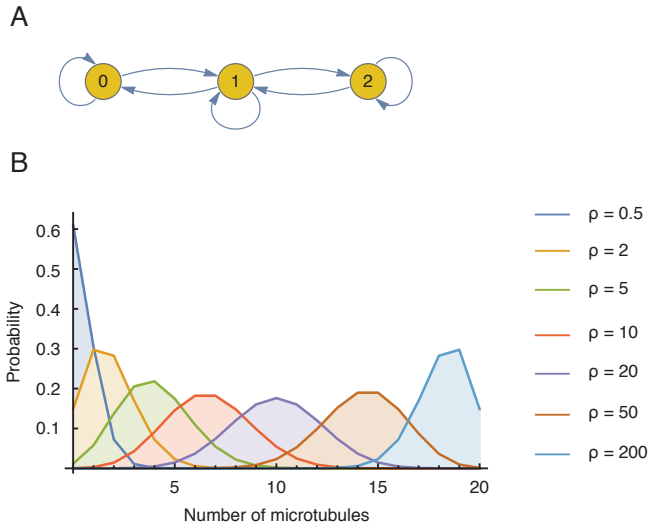

Fig. S1. A basic Markov chain model of kinetochore-microtubule interactions. (A) The Markov chain for $n = 2$. (B) Probability distribution of the number of kMTs (u_k) for $n = 20$ and ρ as indicated. See SI Text for details.

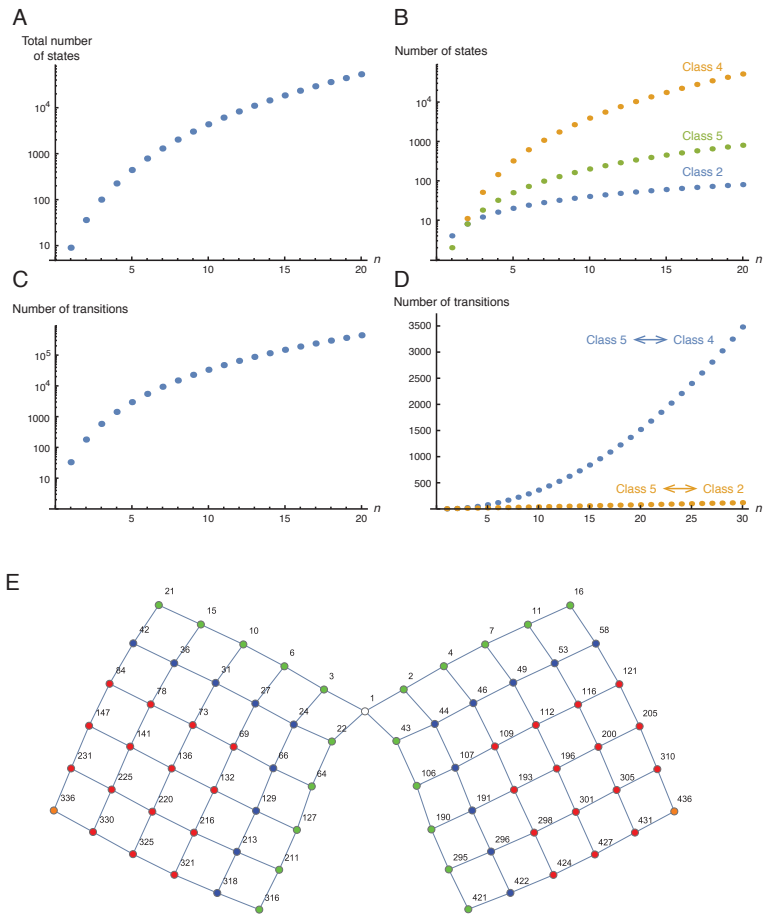

Fig. S2. The size and structure of the Markov chain in the full model (Model III). For details of (A-D), see SI Text. (A) Total number of states. (B) Number of states in each class. Note that Class 3 and 5 have the same number of states. (C) Number of possible transitions. (D) Number of possible transitions in and out of class 5. (E) Graph of class 1, 2 and 5 for $n = 5$. All edges are bi-directional. Numbers indicate the indices of the states. Class 3 and class 4 are omitted. Class 5 (blue, red and orange) consists of two sub-classes corresponding to $r_n(i_1, 0, 0, j_2)$ and $r_n(0, j_1, i_2, 0)$. Two class 5 states (orange) correspond to those with max number of microtubules, i.e. $r_n(0, n, n, 0)$ and $r_n(n, 0, 0, n)$. Class 2 states are marked in green. Class 5 states can communicate with both class 2 and class 4. Note that every state in class 5 (red and blue) but two (orange) directly communicates with class 4. In contrast, only a minor fraction of class 5 (blue) can communicate directly to class 2, which are at the 'periphery' of the class 5 chain. Note that the amphitelic states in blue has $i = 1$ and/or $j = 1$, i.e. either of the kinetochores has only a single microtubule attached. As n grows, so do the two square lattices of the chain. But this graph structure remains the same.

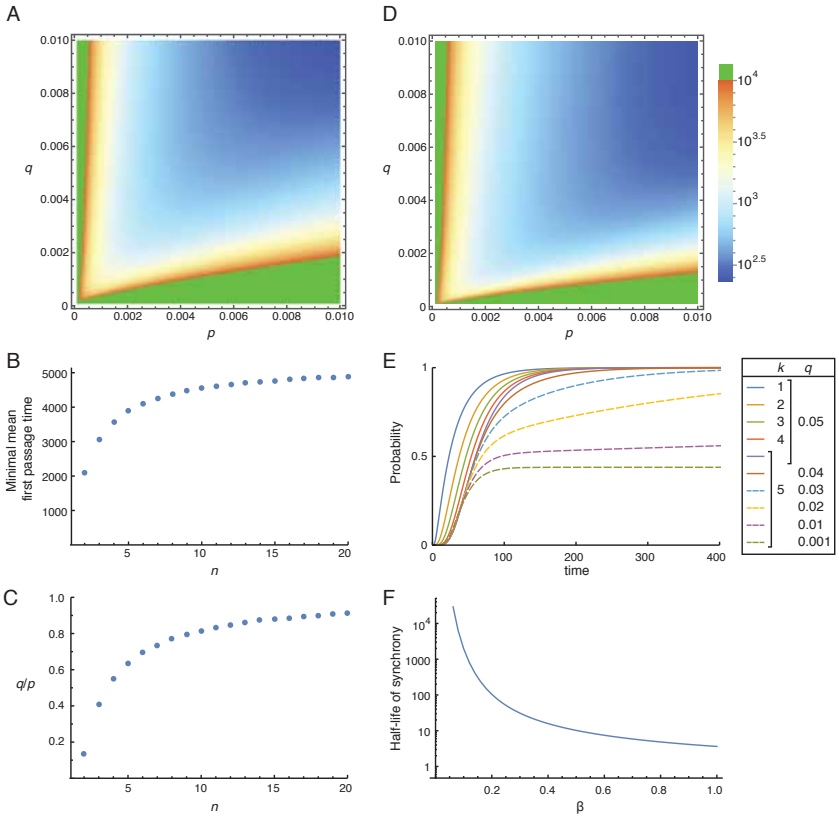

Fig. S3. Chromosome bi-orientation in meiosis and mitosis. (A) A density plot of mean first passage time to class 5 in meiosis I. n =10. Green indicates >10,000. (B, C) The minimum mean first passage time in meiosis I (B) and the corresponding q/p ratio (C) for a fixed value of q (= 0.0005) plotted as a function of n. q/p approaches 1 while the minimum first passage time plateaus as n grows. (D) A density plot of the mean first passage time in mitosis. (E) Probabilities of synchrony in mitosis over time. k = number of pairs of sister chromatids, $p = 0.05$, $\beta = 0$. (F) Half-life of synchrony at steady states in mitosis. $k = 5$, $p = q = 0.05$. β needs to be small to maintain synchrony. In (D, E, F), n =10, $\alpha = 0$ and $\gamma = 0.1$.

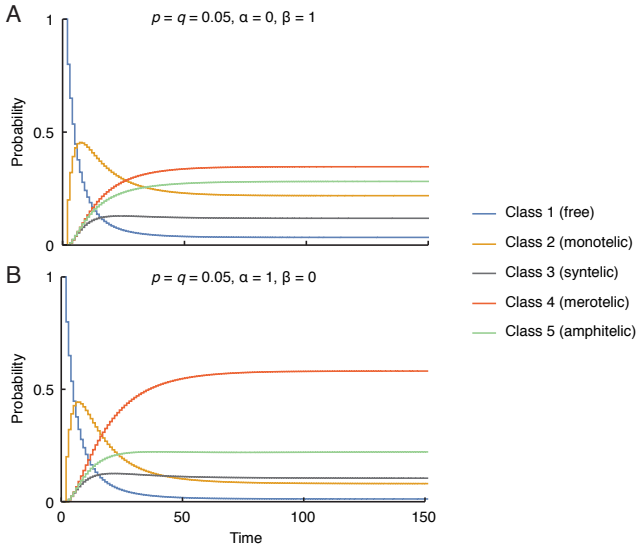

Fig. S4. Probability change of each class over time in meiosis I. (A) $\alpha = 0, \beta = 1$. (B) $\alpha = 1, \beta = 0$. The other parameter values are $n = 10, p = q = 0.05$.

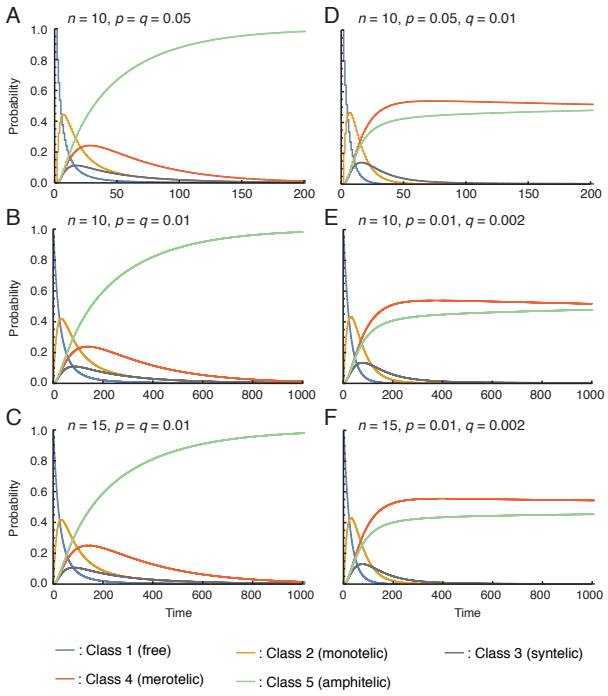
A
n = 10, p = q = 0.05
D
n = 10, p = 0.05, q = 0.01
B
n = 10, p = q = 0.01
E
n = 10, p = 0.01, q = 0.002
C
n = 15, p = q = 0.01
F
n = 15, p = 0.01, q = 0.002
Probability
Time
: Class 1 (free)
: Class 2 (monotelic)
: Class 3 (syntelic)
: Class 4 (merotelic)
: Class 5 (amphitelic)

Fig. S5. Invariant dynamics of the Markov process with a constant *q*/*p* ratio. Examples of PMF time series (meiosis I) are shown. $\alpha = \beta = 0$ for all panels. Other parameters are as indicated. The dynamics are almost indistinguishable for a given q/p ratio besides the difference in time scale. Even with different n, they are qualitatively very similar (B versus C, or E versus F). See SI for details.

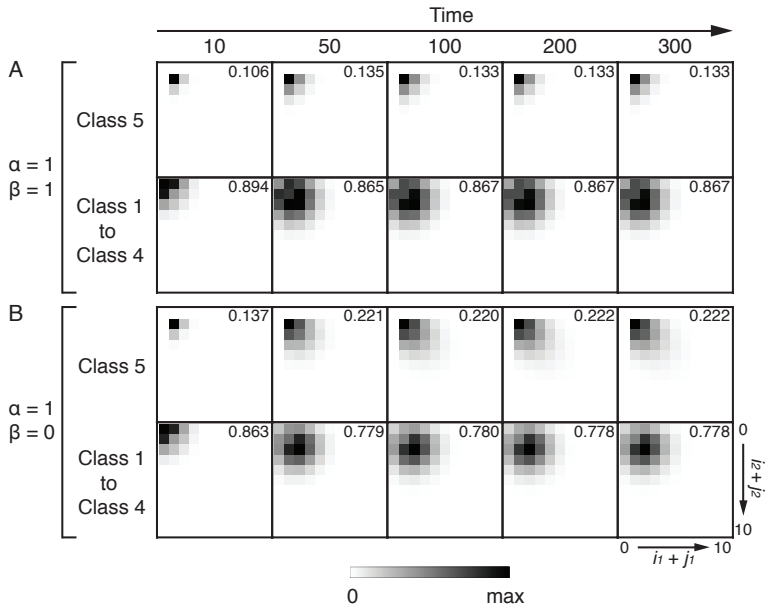

Fig. S6. Probability distribution of the number of kMTs over time in meiosis I.
The probability distributions of the kMT number are shown as density plots. Total probability of class 5 and class 1 to 4 are indicated on each panel. Parameters: $n = 10, p = q = 0.05$; α, β values are indicated on the left. kMT number distribution remains low (unstable) with $\alpha = 1$.

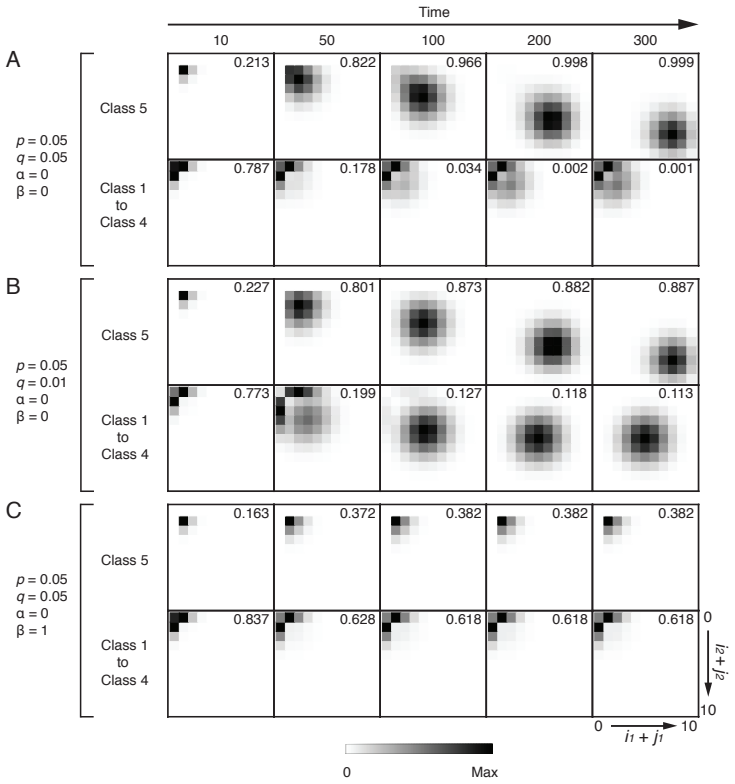

Fig. S7. Probability distribution of the number of kMTs over time in mitosis. Probability density plots of kMT numbers in 2D ($i_1 + j_1$ vs. $i_2 + j_2$; see Fig. 1C) at the indicated time points. Parameters are indicated on the left for each panel; $n = 10$ and $\gamma = 0.1$ for all panels. Probabilities are decomposed into class 5 and the rest (class 1 to 4) at each time point, Total probabilities are indicated on each panel. The densities are scaled from 0 to the maximal in each panel.

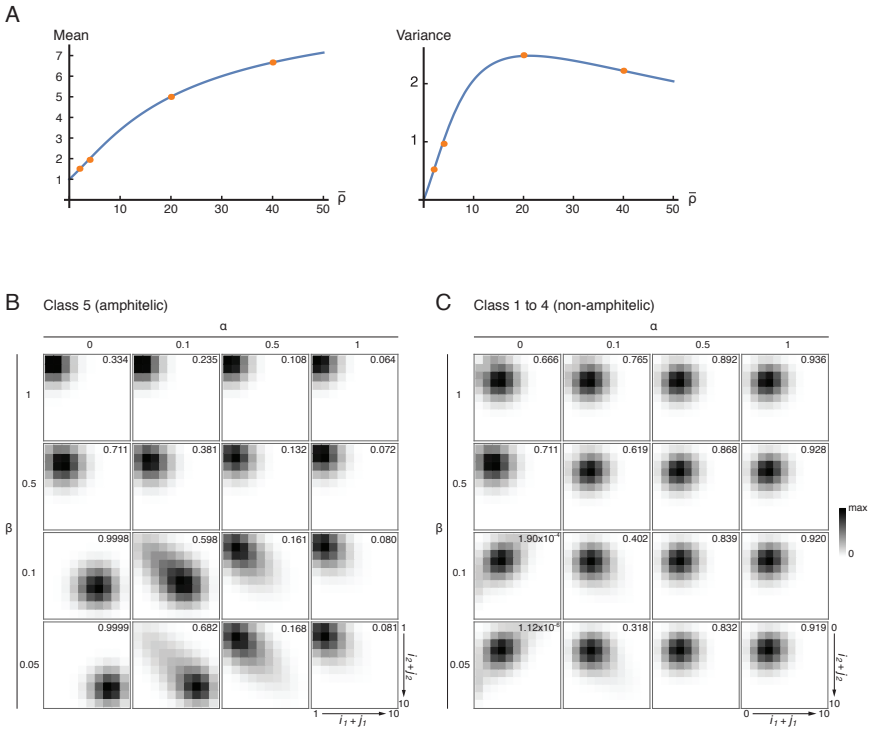

Fig. S8. Distribution of the number of kMTs at steady states. (A) An analytical approximation of kMT number in class 5 when $\alpha = 0$ at steady states. Orange indicates the sample points of the exact kMT numbers (mean and variance) derived from the steady-state PMF and blue curves the functions of approximation according to Eqs. (3) and (10). See SI Text for the derivation of the approximation. Parameters: $n = 10$, $p = 0.05$, $q = 0.05$. (B, C) The probability distributions of kMT number in meiosis I with the indicated parameters α and β are shown as density plots. Total probabilities of class 5 (B) and class 1 to 4 (C) are indicated on each panel. Parameters: $n = 10$, $p = 0.1$, $q = 0.05$.

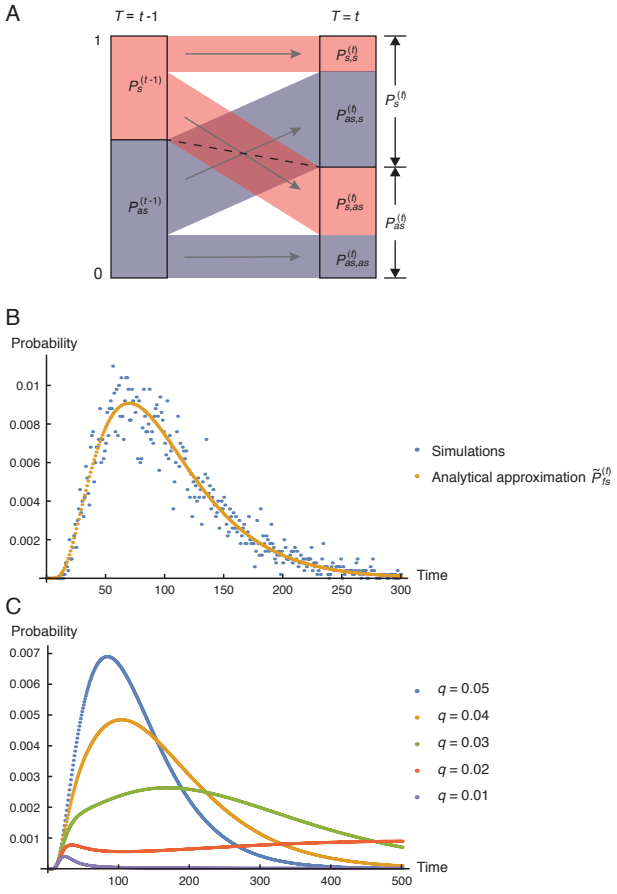

Fig. S9. Approximation of the probability of first synchrony. (A) Diagram of probability change of synchrony and asynchrony in each time step. For details, see SI Text section 'Probability of synchrony'. (B) Analytical approximation of the probability of first synchrony (yellow) together with Monte Carlo simulation results (blue dots; probability at each time point in 5,000 simulations) is shown. Parameters: $n = 5$, $p = q = 0.05$, $\alpha = \beta = 0.01$. (C) Timing of the first synchrony with reducing q/p ratio. The plot shows the probability of the first synchrony at every time points in different conditions as indicated. As q/p ratio declines, the timing of first synchrony spreads more and more over time, becoming unpredictable. Parameter values: $n = 10$, $p = 0.05$, $\alpha = \beta = 0.05$ and number of bivalents (Markov processes) $k = 5$; $\gamma = 1$ (meiosis I).

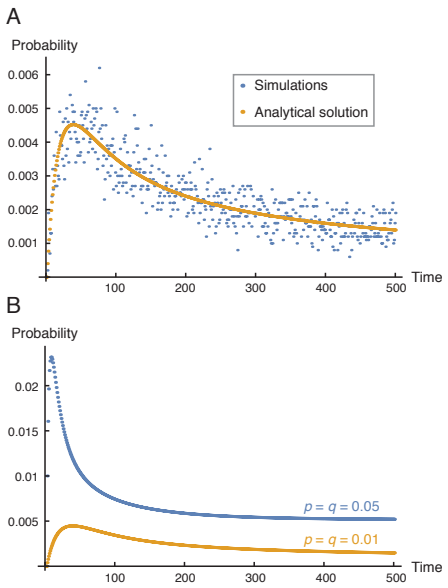

Fig. S10. Probability of bi-orientation attempts. (A) An analytical solution (yellow) and the probabilities of bi-orientation attempts obtained from simulations (blue dots; probability at each time point in 10,000 simulations) is shown. Parameters: $n = 5$, $p = q = 0.01$, $\alpha = \beta = 0.1$. This demonstrates a good fit of the analytical solution to the data obtained by simulations. (B) Probability time series of bi-orientation attempts. Parameters: $n = 10$, $\alpha = \beta = 0.1$. Bi-orientation attemps are more frequent with $p = q = 0.05$ than with $p = q = 0.01$. The probability of bi-orientation attempts at steady states (at any time point) decreases from ~0.033 with $p = q = 0.05$ to ~0.0066 with $p = q = 0.01$. See SI Text for the derivation of the analytical solution.